



Effect of Ce Addition on the Tribological Behavior of ZK60 Mg-Alloy

S. M. Banijamali¹ · Y. Palizdar² · S. Najafi³ · A. Sheikhani³ · M. Soltan Ali Nezhad² · P. Valizadeh Moghaddam⁴ · H. Torkamani^{3,4}

Received: 31 May 2020 / Accepted: 16 July 2020 / Published online: 6 August 2020
© The Author(s) 2020

Abstract

The present work aims to study the tribological behavior of an extruded ZK60 alloy in the presence of Ce; in a previous study, among ZK60 alloys with different Ce addition rates, an alloy with 3 wt% of Ce was found to exhibit the most promising mechanical (e.g., hardness and strengths) properties, while its wear behavior remained unknown. The results of microstructural examinations by optical and electron microscopes show that Ce addition reduces the grain size from 6.1 to 2.0 μm . Besides, in addition to the precipitates already distributed in the base alloy (Mg_7Zn_3), Ce could promote the formation of a new precipitate (MgZn_2Ce), increasing the total fraction of the precipitates. These microstructural evolutions enhance the strengths of the studied ZK60 alloy, as the yield and tensile strengths increase from 212 to 308 MPa and from 297 to 354 MPa, respectively. A pin on disc tribometer was employed to study the wear behavior of the developed alloy under different normal loads (5, 20, 40, and 60 N). The results show that the base and Ce-added alloys exhibit almost a similar frictional behavior, while the wear resistance of the Ce-added alloy is higher within the load ranges applied: (i) in low load conditions (5 and 20 N), where the abrasive wear is the active mechanism, the precipitates in the Ce-added alloy could enhance the wear resistance. (ii) Under the load of 40 N, oxidative wear is also an operative wear mechanism, leading to a sharp increase in the wear rate of the alloys. In this condition, Ce could provide a protective oxide layer, which could improve the wear resistance of the alloy. (iii) At a load of 60 N, both studied alloys exhibit a similar wear rate due to a severe oxidation condition. Therefore, beyond this loading condition, the microstructural evolutions (e.g., change in precipitation behavior) caused by Ce addition can no longer contribute to the enhancement of wear resistance.

Keywords ZK60 magnesium alloy · Ce addition · Pin on disc · Abrasive wear

1 Introduction

Magnesium alloys have attracted considerable attention due to their high specific buckling resistance, good castability, low density, and good damping capacity, making them suitable for some applications such as automotive industries, aircraft structures, and other lightweight structural components [1]. However, their relatively low strength and weak tribological behavior have limited the potential applications of these alloys. Thus, researchers have recently focused on improving the mechanical properties and wear resistance of the magnesium alloys [2–7]. In this regard, various techniques have been employed so far in order to enhance the strength of these materials. Alloying can be considered as an effective way to strengthen the alloys; for instance, the addition of Zn and Zr to Mg alloys could enhance their strength [8]. Apart from the common alloying elements, it has been

✉ Y. Palizdar
y.palizdar@merc.ac.ir

H. Torkamani
hadi.torkamani@ltu.se

¹ Faculty of Mechanical Engineering, K. N. Toosi University of Technology, P.O. Box 15875-4416, Tehran, Iran

² Department of Nano-technology and Advanced Materials, Materials & Energy Research Center (MERC), Karaj 3177983634, Iran

³ School of Metallurgy and Materials Engineering, College of Engineering, University of Tehran, P.O. Box 11155-4563, Tehran, Iran

⁴ Materials Science Division, Department of Engineering Sciences and Mathematics, Luleå University of Technology, 97187 Luleå, Sweden

demonstrated that the addition of Rare Earth elements (RE) such as Y, Nd, Ce, Ca, and Gd to Mg alloys would result in a remarkable improvement in strength and creep properties at elevated temperatures due to the formation of thermally stable intermetallic compounds [9–14]. Chia et al. [10] studied the influences of La, Ce, and Nd additions into a commercially pure Mg. They showed that the mechanical properties could be affected by the type, volume fraction, and morphology of the intermetallic phases. It has been reported elsewhere that the tensile behavior of Mg–Zn–Zr alloy is significantly improved by RE addition (Y and Ce), which is due to the grain refinement and formation of different intermetallic phases [12, 15].

There are other published reports in the literature investigating the effects of different microstructural parameters on the wear resistance of Mg alloys [16–22]; only a few reports are dedicated to the effects of RE on the tribological behavior of Mg alloys. For instance, Hu et al. [19] observed that the amount of $Mg_{12}Y_1Zn_1$ phase, surface oxidation, and retained wear debris could affect the wear rate of the alloy where abrasion and plastic deformation have been the main wear mechanisms in dry sliding condition. It has been reported elsewhere that the addition of Ce-rich misch metal to AZ91 alloy results in the formation of an intermetallic phase, leading to enhancement of high temperature creep resistance and wear behavior of the alloy tested against a tool steel. Abrasion, delamination, and gross plastic deformation were considered as the dominant wear mechanisms in that work [18]. Nouri et al. [23] showed that the formation of a hard second phase (Al_2Y ; in the presence of Y in Mg–3%Al alloy) could improve the wear resistance. The effect of Al_2Y on the wear property of Mg–3%Al–1%Zn alloy was also reported by Sun et al. [24]. Zengin et al. [16] studied the effect of minor Nd addition on the mechanical and tribological behavior of ZK60 alloy, which led to notable grain refinement, improving both tensile strength and ductility of the alloy.

Having reviewed the published reports, one can realize that there is a lack of information regarding the correlation between the microstructural features and tribological behavior of Mg alloys, especially in the presence of RE elements. In a recent work of the authors, a new ZK60 alloy containing 3 wt% Ce has been developed [25], where it was demonstrated that Ce addition could affect the precipitation manner and refine the microstructure, resulting in higher strengths compared to the base alloy. In the current study, attempts have been made to unveil the link between the microstructural features and wear property in the developed Ce-added alloy.

2 Materials and Experimental Procedures

2.1 Materials and Processing

To investigate the effects of Ce addition on the microstructure and wear behavior of Mg alloys, 3 wt% of Ce was added to a base ZK60 alloy; two ZK60 alloys with a similar base composition were produced, while one of them contains Ce. In a previous work of the authors, it has been found out that the alloy containing 3 wt% Ce possesses the most promising mechanical properties in terms of hardness and strength levels [25], while the wear behavior of the developed alloy remained unknown.

High purity Mg (99.9 wt%), Zn (99.9 wt%), and Mg–30 wt% Zr + Mg–30 wt% Ce master alloys were used to produce the targeted alloys. An induction furnace (model: IGM12-3) was used to melt the raw materials. Mg was first placed in the graphite crucible with a temperature of 740 °C. The Melting process was carried out in a protective atmosphere (a mix of SF₆ and CO₂). Having melted the pure Mg, Zn was added to the melt, which was held and stirred (using a stainless steel rod) for 15 min afterwards. Then, the master alloys were added into the molten alloy. The melt was mechanically stirred again for 2 min to reach a homogenous composition. After a 5-min rest period, the melt was poured into a preheated (200 °C) cylindrical steel mold with a diameter of 30 mm, a height of 45 mm, and a thickness of 2 mm. Inductively Coupled Plasma (ICP, model: VARIAN VISTA-PRO) technique was used to measure the amount of the elements present in the alloys. The chemical composition of the cast alloys is given in Table 1. In this study, the terms ZK60 and ZK60–3Ce refer to the base and Ce-added alloys, respectively.

The cast alloys were machined to a cylindrical shape with a length of 28 mm and 29 mm in diameter. The parts were then homogenized at 440 °C for 12 h to, as much as possible, reduce the compositional inhomogeneity. It has been carried out according to the methodology suggested earlier [25]. The homogenized parts were finally extruded at 440 °C with an 18:1 extrusion ratio.

2.2 Metallography and Microstructural Examinations

The microstructures of the studied alloys were inspected under Optical (OM, Leitz) and Scanning Electron Microscopies (SEM, ZEISS SIGMA VP). For this purpose, metallographic samples were ground and then polished with 0.05 μ alumina suspension. The polished surfaces were

etched using an acetic picric etchant (5 ml ethanol, 1 ml acetic acid, 2 ml distilled water, and 0.4 g picric acid). OM images were randomly taken and analyzed using Digimizer image analyzing software in order to determine the average grain size of the alloys, according to ASTM-112E standard. For each alloy, at least 300 grains were delineated on the OM images without bias.

X-Ray Diffraction (XRD, PHILIPS) and Energy Dispersive Spectroscopy (EDS) techniques were employed to identify the phases present in the microstructure of the alloys. The XRD data was obtained by using Cu-K α radiation operated at 40 kV and tube current of 30 mA over the 2θ ranging from 20° to 80° . A step size of 0.02° , with a counting time of 0.5 s per step, was used to run the XRD tests.

2.3 Mechanical Testing

The hardness of the samples was measured using a WOLPER machine with a Vickers indenter at a force of 0.98 N (dwell time of 30 s). The hardness test was repeated at least five times on each sample, and an average was reported.

The tensile tests were performed on the extruded specimens prepared according to ASTM: E8-04 standard. A SANTAM machine with a capacity of 2 tons and a jaw velocity of 0.1 mm/sec was used to perform the tensile tests. For each alloy/condition, three samples were prepared and tested, and an average was reported.

2.4 Wear Testing

A pin-on-disc tribometer was employed to carry out a dry sliding wear test at room temperature. The pin specimens with dimensions of 5 mm in diameter and 15 mm in height were made from the ZK60 and ZK60-3Ce alloys. The counterpart surface was an AISI52100 steel disc, 40 mm in diameter, and 5 mm in thickness. Before running the wear tests, both disc and pin were cleaned by an ultrasonic cleaner so as to remove any possible traces of contaminants.

To presumably establish the mild, medium, and severe wear conditions, the wear tests were carried out under normal loads of 5, 20, 40, and 60 N. These loading conditions were chosen according to the published reports [26, 27]. A constant sliding speed of 0.5 m/s was set to run the test for a sliding distance of 1000 m. The tribometer recorded the friction coefficient and sliding distance continuously. The samples were weighed before and after the wear tests in order to determine the weight loss. The volume loss during the wear test was determined from the weight loss and the alloy's density.

In addition to the worn surfaces of the pin specimens, the produced wear debris was collected and examined using an SEM (equipped with EDS unit).

3 Results and Discussion

3.1 Microstructural Observation

Figure 1 shows the microstructure of the extruded alloys. As it can be seen in Fig. 1a, the microstructure of the base alloy consists of equiaxed α -Mg grains formed through Dynamic Recrystallization (DRX). Compared to the base alloy, finer grains are obtained in ZK60-3Ce alloy (Fig. 1b). OM images were employed to measure the grain size in both alloys under investigation. The results of grain size measurement show that the grain size of ZK60 alloy is reduced from 6.1 to 2.0 μm when 3 wt% of Ce has been added to the base alloy.

Figure 2 illustrates the SEM images of the extruded alloys. The results of EDS microanalyses of the various precipitates (indicated by the yellow arrow in Fig. 2) are also shown in the tables below their corresponding image. From Fig. 2a, it is apprehended that the microstructure of the base alloy is composed of few Mg-Zn precipitates distributed in a matrix of α -Mg. Figure 2b shows that the fraction of the precipitates (the white spots) significantly increases in the presence of Ce. Some of these precipitates are rich in Ce. Similar observations to Fig. 2 suggest that the volume fraction of the precipitates increases from ~ 1 to $\sim 12\%$ when 3 wt% of Ce has been added to the base alloy.

XRD analysis was carried out in order to identify the precipitates existed in the microstructure of the alloys under investigation. Figure 3 shows that the base alloy is composed of α -Mg and Mg_7Zn_3 precipitates. In agreement with EDS results (Fig. 2), this figure also shows that, in addition to Mg_7Zn_3 , there is a Ce-containing precipitate (MgZn_2Ce) in the microstructure of ZK60-3Ce alloy. In fact, due to the limited solubility of Ce in Mg, this element tends to form new precipitates [17], which, according to XRD results, are identified as MgZn_2Ce . These precipitates have a high melting point and good thermal stability, and they can lock the grain boundaries through the pinning effect [28]. The role of Ce as Particle Stimulated Nucleation (PSN) in Mg alloys can

Table 1 Chemical composition of the materials used in this study (Mg to balance)

Alloy	Elements (wt%)		
	Zn	Zr	Ce
ZK60	6.04	0.49	—
ZK60-3Ce	5.94	0.48	2.96

be regarded as another factor affecting the microstructural components [29]. More explanations of the microstructural evolutions (i.e., precipitation manner and grain refinement) and the phenomena taken place in the presence of RE can be found in our previous work [25].

3.2 Hardness and Tensile Properties

Table 2 shows that the addition of Ce to the base alloy enhances the hardness level (about 10%). This increase in hardness, though slight, could be due to the microstructure refinement as well as a higher volume fraction of the precipitates in ZK60-3Ce alloy. Table 2 also gives the data extracted from the tensile tests for the extruded alloys. It can be seen that the addition of Ce improves the mechanical properties of the studied alloy, as the Yield Strength (YS) and Ultimate Tensile Strength (UTS) increase from 212 to 308 MPa and from 297 to 354 MPa, respectively. The enhancements in the YS and UTS are attributed to the microstructural evolutions achieved by Ce addition. According to Hall-Patch relation, grain refinement results in enhancements in the strengths of the materials [30]. Ce addition could also promote the formation of new precipitates in the studied alloy, increasing the total fraction of the precipitates. Apart from the direct effect of these precipitates on the hardness and strengths, they would have a pinning effect on the grain boundaries, causing further refinement [31, 32]. The decrease in the elongation (Table 2) could be due to the larger volume fraction of precipitates formed in the ZK60-3Ce alloy. Because, as stress concentration sites, they might lead to a premature failure during the hot extrusion or tensile test, decreasing the elongation of the alloy [33]. The correlation between the microstructure and mechanical properties of similar alloys has been deeply studied in our previous work [25].

3.3 Wear Behavior

3.3.1 Friction Coefficient

Figure 4 shows the steady-state friction coefficients under different normal loads. It can be seen that there is no significant difference between the friction coefficient of ZK60 and ZK60-3Ce alloys, as it lies within a range of 0.12 to 0.26.

The results of friction coefficient as a function of sliding distance under the normal loads of 5, 20, 40, and 60 N for ZK60-3Ce alloy are shown in Fig. 5. It can be seen that the oscillations around the mean value are different when different loads have been applied to the specimens. For instance, at a load of 5 N, the friction coefficient exhibits a more unstable behavior compared to the other normal loads. This can be attributed to the formation and breakage of adhesive junctions between the pin and disc, leading to a sudden increase and drop in the tangential force and friction coefficient. At the low load range (5 N), a uniform and stable oxide layer cannot form on the worn surface, and thus, metal to metal contact can be established. At higher load regimes, formation of an oxide layer (due to higher contact temperature) can prevent the metal to metal contact, resulting in a more stable coefficient of friction.

3.3.2 Wear Rate

The results of volumetric wear rates as a function of applied load for ZK60 and ZK60-3Ce alloys are shown in Fig. 6. It seems that the volumetric wear rate of both alloys increases as the normal load increases. Furthermore, the ZK60-3Ce alloy shows a lower wear rate than the ZK60 alloy within all the different applied loads. This implies that the presence of new precipitates and grain refinement caused by the Ce

Fig. 1 Optical micrographs of the extruded **a** ZK60 and **b** ZK60-3Ce alloys

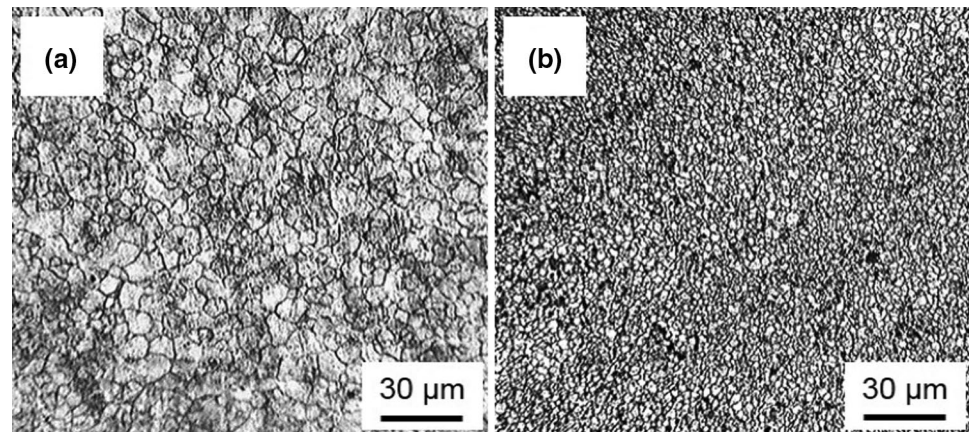


Fig. 2 SEM micrographs and EDS microanalysis results of the precipitates distributed in the microstructure of **a** ZK60 and **b** ZK60-3Ce specimens

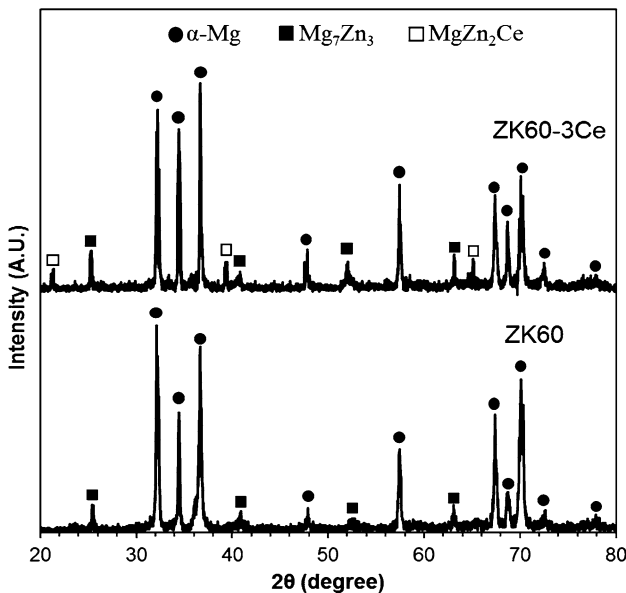
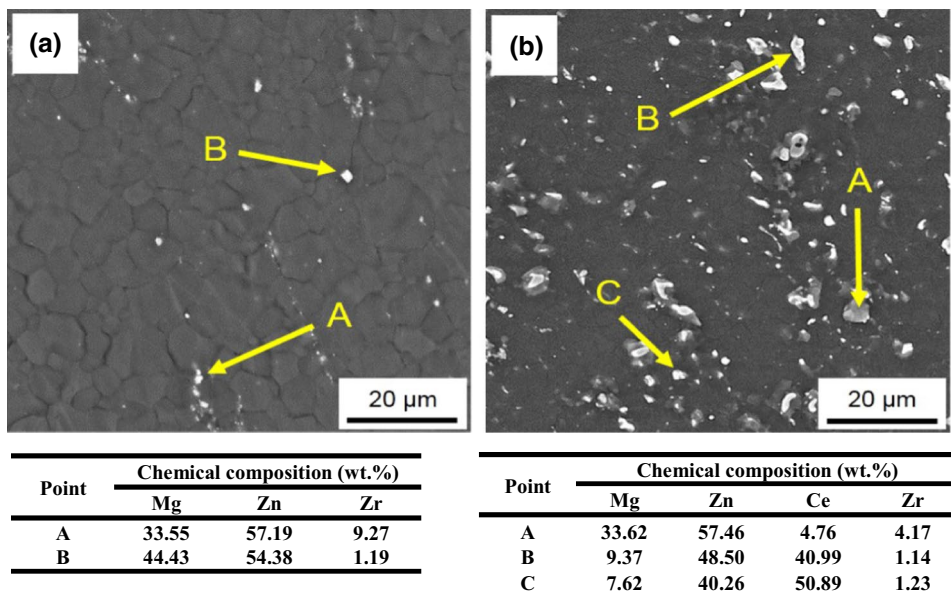


Fig. 3 XRD results identifying the phases existed in the microstructure of the extruded specimens

addition to the base ZK60 alloy can be effective in reducing the wear rate. As it can be observed in Fig. 6, ZK60-3Ce alloy exhibits similar wear rates at loads of 5 and 20 N (wear rate of ZK60-3Ce alloy is not significantly affected by increasing the normal load from 5 to 20 N). However, there is a sharp increase in wear rate of ZK60-3Ce alloy when the normal load increases from 20 to 40 N. Hence, there is a transition from mild wear to severe wear in these

Table 2 Mechanical properties of the studied alloys

Alloy	Vickers hardness (HV)	UTS (MPa)	YS (MPa)	Elongation %
ZK60	80±2	297±8	212±7	30±2
ZK60-3Ce	88±2	354±8	308±9	20±1

load regimes, where the wear rate of the Ce-added alloy is still lower than the base one. By increasing the normal load to 60 N, both alloys demonstrate a similar wear rate. This somehow implies that Ce addition cannot be effective in reducing the wear rate at a high load (60 N).

3.3.3 Wear Mechanisms

In order to understand the wear mechanisms operating at different normal loads, the worn surfaces of the pin specimens were analyzed by the scanning electron microscope. Figure 7 shows the SEM images of the worn surfaces along with the results of EDS corresponding to the selected areas within each image. Figure 7a, b display the worn surface of both Mg-alloys tested at a load of 5 N. There are numerous grooves and scratches running parallel to the sliding direction, indicating the abrasive wear mechanism [34–36]. These grooves are typically caused by the hard asperities on the steel counterpart or by the generated wear particles in the contact region which plow or cut the soft surface of the magnesium specimens. Regarding the latter case, the generated wear particles can be severely

deformed and oxidized during the wear process, which exhibit higher hardness than the base Mg-alloys and can cause further abrasion. Thus, the abrasive mechanism is considered as the dominant wear mechanism at the lower normal loads (i.e., 5 N).

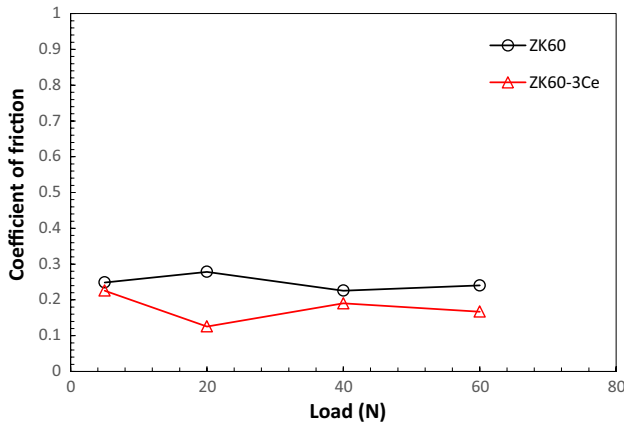
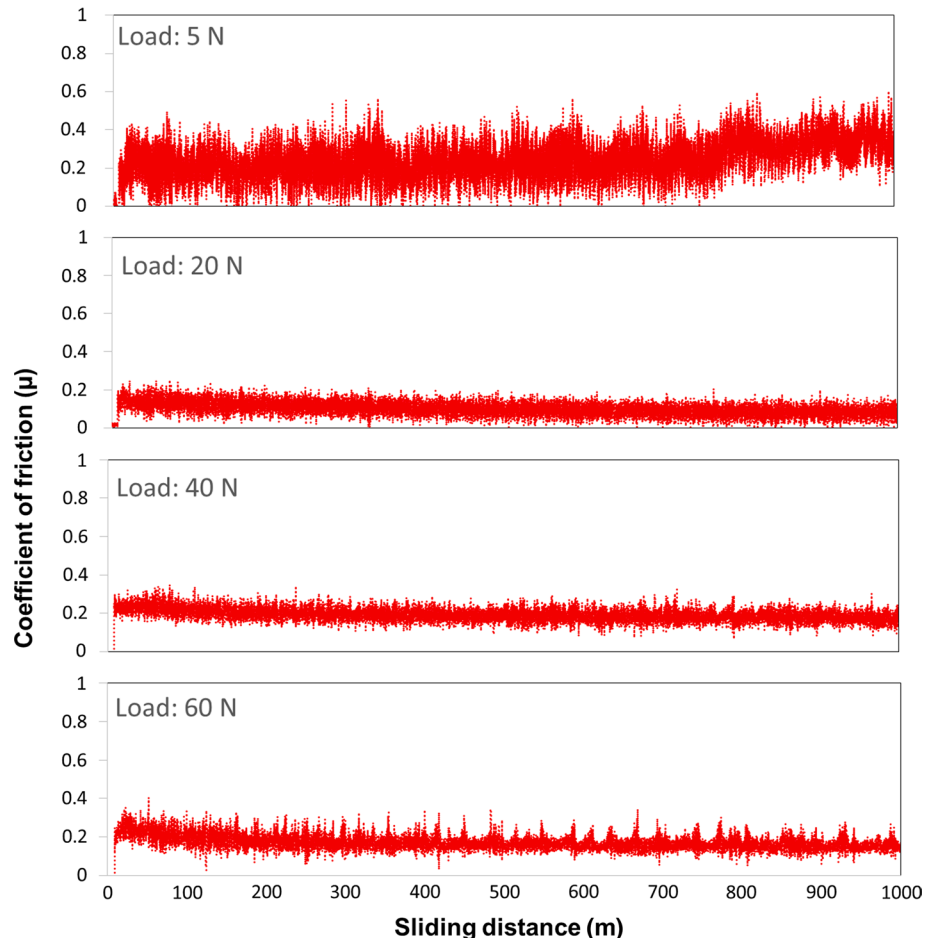


Fig. 4 The average steady-state friction coefficient as a function of normal load

Fig. 5 The evolution of friction coefficient with sliding distance under different normal loads for ZK60-3Ce alloy



The parallel grooves observed in Fig. 7c and d indicate that the abrasive wear is also the prevailing wear mechanism at a load of 20 N. Figure 7c shows that the width of the grooves on the worn surface can increase with an increase in the normal load. At a higher load (20 N), the depth of penetration by the hard asperities of the counterpart increases, as a consequence, a larger volume of material can be removed through the micro-cutting mechanism. In this way, the wear rate of the specimens increases with increasing the normal load (Fig. 6). The presence of Ce-containing precipitates in ZK60-3Ce alloy (Figs. 2 and 3) can improve the abrasive wear resistance by providing effective barriers to the plastic deformation [35]. Moreover, higher yield and ultimate tensile strengths obtained for ZK60-3Ce alloy (Table 2), as results of the grain refinement and formation of precipitates, can further contribute to the improvement of the abrasive wear resistance. Therefore, the width of the grooves and wear rate of ZK60-3Ce alloy does not significantly increase with increasing the normal load from 5 to 20 N.

The appearance of the worn surfaces that experienced a load of 40 N (Fig. 7e and f) is quite different from those that have been subjected to lower loads of 5 and 20 N (Fig. 7a–d). As indicated in Fig. 7e and f, the spallation of the studied

Mg-alloys can take place during the wear process. The results of the EDS analysis on the spalled region reveal high oxygen contents, suggesting that the oxidative wear mechanism can occur when a higher load (40 N) has been employed. During the wear process, the contact temperature can increase with increasing the normal load. Therefore, the Mg-alloys can be readily oxidized at higher contact temperature in the ambient atmosphere. Consequently, the oxidized patches can be formed on the worn surface [26, 37]. These oxidized patches are brittle and can be easily detached, leaving a spalled region on the worn surface. In addition to oxidative wear, abrasion can also take place at this load by either the harder asperities of counterpart or the produced wear debris. Therefore, the sharp increase in the wear rate observed in Fig. 6 (where the load increases from 20 to 40 N) can be attributed to the change in the active wear mechanisms. Figure 8 shows the details of fracture and crack formation on the oxidized patches corresponding to the load of 40 N. The magnified images shown in this figure intend to provide more details on the spalled region.

The oxidized layer on the worn surface can reduce the metal to metal contact [22, 26]. Thus, a more stable coefficient of friction can be observed at the higher loads (Fig. 5). Comparing Fig. 7e and f, one can say that the size of the oxidized patch in the ZK60 alloy is significantly larger than that in the ZK60-3Ce alloy. This implies that the presence of MgZn₂Ce precipitates is effective in reducing the size of the fractured oxidized patches and thereby the wear rate. In this regard, Liu et al. [38] reported that the oxide film formed on the surface of ZK60 alloy contains a number of defects that allow the growth of oxide. Therefore, during the wear process, a loose and cracked

oxide layer on the surface of ZK60 alloy can be easily fractured [38]. On the other hand, several studies [39–41] reported that Ce in Mg-alloys could increase the resistance to the oxidation of Mg-alloy. The addition of Ce to Mg-alloys leads to formation of a protective and compact oxide layer on the surface during the wear process. This uniform oxide layer can hinder the further growth of oxide, making it less susceptible to fracture and spallation (Fig. 8). This can explain the higher wear rate of ZK60 alloy compared to the ZK60-3Ce alloy at a load of 40 N.

The worn surface of the ZK60 and ZK60-3Ce alloys tested at a load of 60 N is illustrated in Fig. 7g and h, respectively, which can be characterized by both grooves and fractured regions. The results of EDS analyses show high oxygen contents on the worn surface of both alloys. This suggests that oxidation can easily take place at higher load due to higher contact temperature. As indicated in Fig. 7g and h, during the wear process, cracks can initiate and propagate at the oxidized region, leaving a fractured region on the worn surface. Eventually, these oxidized regions spall off from the surface and form the sheet-like wear debris. Subsequently, the produced wear debris can act abrasively. Moreover, at a load of 60 N, the precipitates can no longer be effective in reducing the abrasion, and the wear rates of both alloys are quite similar.

To support the explanations on the active wear mechanisms provided up to here, the wear debris of the ZK60-3Ce alloy has been studied under the SEM. Figure 9 shows the morphology of the debris collected after the wear tests at different loads. At a load of 5 N, the wear debris mainly consists of small oxidized particles (Fig. 9a). The results of EDS analysis on the generated wear particles shown in Fig. 9a confirm the oxidation of the wear particles during the wear process. It can be seen in Fig. 9b that the wear debris generated at a load of 20 N is a mixture of small fragmented and flaky particles. However, at higher loads (i.e., 40 and 60 N), the examination of the wear debris reveals numerous flakes or sheets, indicating the delamination of oxidized patches (Fig. 9c, d). The detachment of this plate-like debris causes an increase in the wear rate of ZK60-3Ce alloy tested at the load of 40 N (Fig. 6); during the wear process, cracks initiate at the subsurface, gradually grow parallel to the sliding direction and eventually reaches the surface. This, in turn, leads to formation of the long thin sheet-like wear debris (Fig. 9c) [34].

Figure 9d indicates that the size of the sheet-like wear debris significantly increases when the normal load increases from 40 to 60 N. This can explain the higher wear rate observed at a load of 60 N. Furthermore, as it is shown in Fig. 9d, the surface of the sheet-like wear debris contain numerous cracks, which can be broken down into smaller particles and cause abrasion during the wear process.

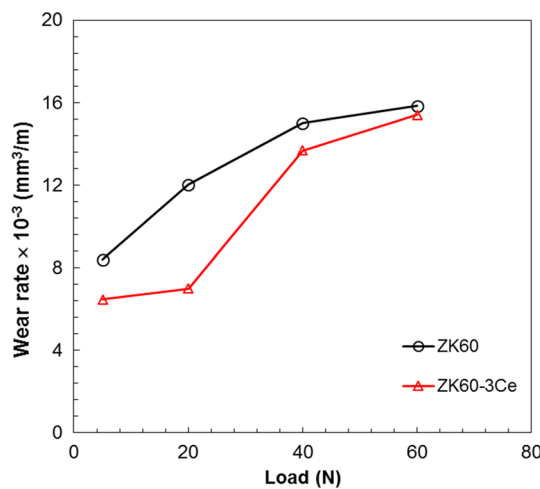


Fig. 6 The results of the volumetric wear rate as a function of applied load for ZK60 and ZK60-3Ce alloys

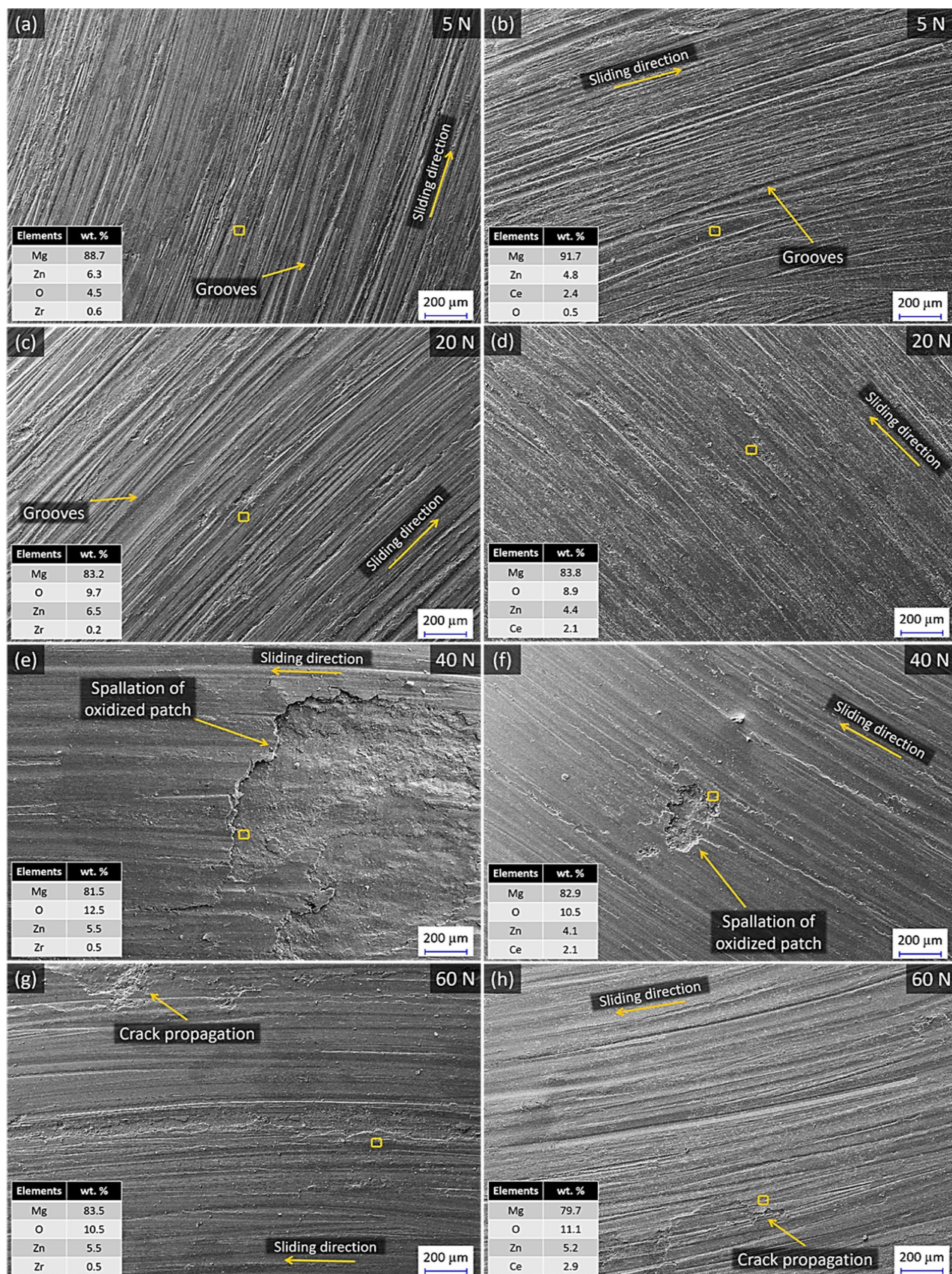


Fig. 7 SEM micrographs and EDS analyses of the worn surfaces of the studied alloys: **a, c, e** and **g** ZK60 alloy, **b, d, f**, and **h** ZK60-3Ce alloy

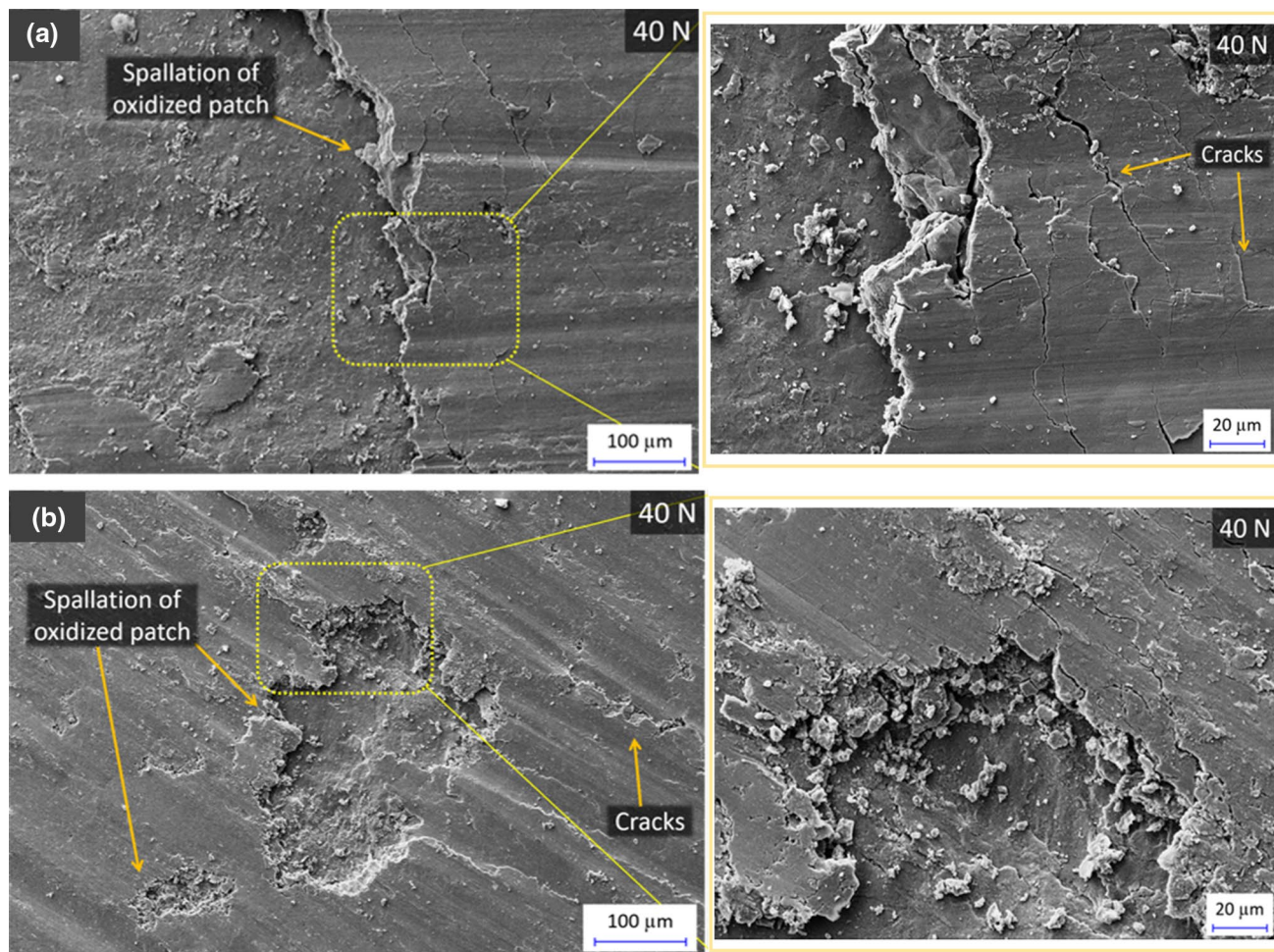


Fig. 8 The details of the spalled oxidized patches on the worn surfaces of **a** ZK60, **b** ZK60-3Ce alloys, at a load of 40 N

4 Conclusions

This study investigated the effect of Ce addition (3 wt%) on the wear behavior of ZK60 extruded alloy under different normal loads. The results of this study are summarized as follows:

1. Ce addition could refine the grain size of the studied alloy from 6.1 to 2.0 μm. It was also found that, in addition to Mg₇Zn₃ which already existed in the microstructure of the base alloy, Ce addition promotes the formation of a new type of precipitates (MgZn₂Ce), increasing the total fraction of precipitates.
2. The addition of Ce could improve the mechanical properties of the ZK60 alloy in terms of yield and ultimate tensile strengths. This can be attributed to the increase in the volume fraction of precipitates and the grain refinement caused by Ce addition.

3. Both studied alloys exhibited similar frictional behavior, while the wear resistance of the Ce-added alloy was higher within the different applied loads.
4. Under the normal loads of 5 and 20 N, the precipitates, fraction of which is higher in Ce-added alloy, could act as deformation barriers, enhancing the abrasive wear resistance of the alloy. When the normal load increased to 40, the surface oxidation also occurred, leading to a sharp increase in the wear rate of the studied alloy. In this condition, it seems that Ce addition could establish a more stable and protective oxide layer, resulting in higher wear resistance compared to the base alloy.
5. Increasing the normal load to 60 N, both studied alloys show a similar wear behavior due to severe oxidative wear condition, where the precipitates could not contribute to the improvement of the wear resistance.

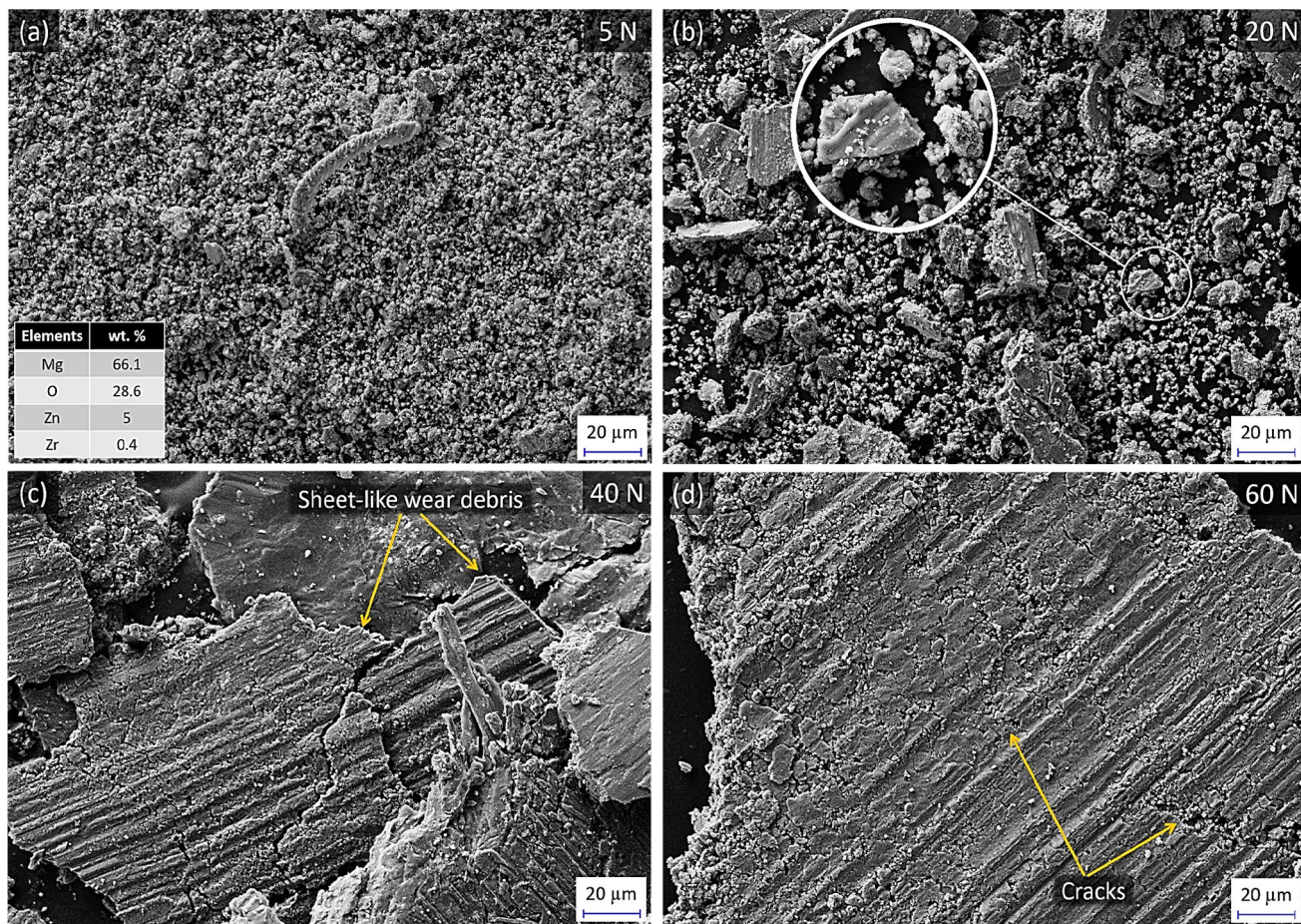


Fig. 9 SEM micrograph of the wear debris detached from ZK60-3Ce alloy, under the different normal loads: **a** 5 N, **b** 20 N, **c** 40 N and **d** 60 N

Acknowledgments Open access funding provided by Lulea University of Technology.

Open Access This article is licensed under a Creative Commons Attribution 4.0 International License, which permits use, sharing, adaptation, distribution and reproduction in any medium or format, as long as you give appropriate credit to the original author(s) and the source, provide a link to the Creative Commons licence, and indicate if changes were made. The images or other third party material in this article are included in the article's Creative Commons licence, unless indicated otherwise in a credit line to the material. If material is not included in the article's Creative Commons licence and your intended use is not permitted by statutory regulation or exceeds the permitted use, you will need to obtain permission directly from the copyright holder. To view a copy of this licence, visit <http://creativecommons.org/licenses/by/4.0/>.

References

- M.K. Kulekci, Int. J. Adv. Manuf. Technol. **39**, 851 (2008)
- Q. Chen, K. Li, Y. Liu, Z. Zhao, K. Tao, Q. Zhu, J. Mater. Res. **32**, 2161 (2017)
- A.K. Mondal, S. Kumar, Wear, **267**, 458 (2009)
- A.W. El-Morsy, Mater. Sci. Eng., A **473**, 330 (2008)
- L. Li, J. Feng, C. Liang, J. An, Materials **11**, 1735 (2018)
- Z. Yang, M. Wei, Y. Zhao, S. Wang, Trans. Nonferrous Met. Soc. China **21**, 2584 (2011)
- D. Liu, M. Shen, Y. Tang, Y. Hu, L. Zhao, Met. Mater. Int. **25**, 1182 (2019)
- W. Cui, L. Xiao, W. Liu, G. Wu, X. Wang, Z. Li, J. Mater. Res. **33**, 733 (2018)
- C. Ma, M. Liu, G. Wu, W. Ding, Y. Zhu, Mater. Sci. Eng., A **349**, 207 (2003)
- T.L. Chia, M.A. Easton, S.M. Zhu, M.A. Gibson, N. Birbilis, J.F. Nie, Intermetallics **17**, 481 (2009)
- A.R. Wu, C.Q. Xia, Mater. Des. **28**, 1963 (2007)
- L. Liu, X. Chen, F. Pan, Z. Wang, W. Liu, P. Cao, T. Yan, X. Xu, Mater. Sci. Eng., A **644**, 247 (2015)
- B. Chen, C. Lu, D. Lin, X. Zeng, Met. Mater. Int. **20**, 285 (2014)
- H. Cia, F. Guo, J. Su, Mater. Res. Express **5**, 016503 (2018)
- E.P. Silva, F. Marques, T.S. Nossa, U. Alfaro, H.C. Pinto, Mater. Sci. Eng., A **723**, 306 (2018)
- H. Zengin, Y. Turen, M.E. Turan, Mater. Res. Express **6**, 086528 (2018)
- H. Yu, S.H. Park, B.S. You, Y.M. Kim, H.S. Yu, S.S. Park, Mater. Sci. Eng., A **583**, 25 (2013)
- K.M. Asl, A. Masoudi, F. Khomamizadeh, Mater. Sci. Eng., A **527**, 2027 (2010).
- M.L. Hu, Q.D. Wang, C. Li, W.J. Ding, Trans. Nonferrous Met. Soc. China **22**, 1918 (2012)

20. S. Anbu Selvan, S. Ramanathan, J. Alloys Compd. **502**, 495 (2010)
21. A. Zafari, H.M. Ghasemi, R. Mahmudi, Mater. Des. **54**, 544 (2014)
22. A. Zafari, H.M. Ghasemi, R. Mahmudi, Wear **303**, 98 (2013)
23. M. Nouri, X. Sun, D.Y. Li, Tribol. Int. **67**, 154 (2013)
24. X. Sun, M. Nouri, Y. Wang, D.Y. Li, Wear **302**, 1624 (2013)
25. A. Sheikhani, Y. Palizdar, M.S.A. Nezhad, S. Najafi, H. Torkamani, Mater. Res. Express **6**, 086594 (2019)
26. F. Labib, H.M. Ghasemi, R. Mahmudi, Wear **348–349**, 69 (2016)
27. A. Zafari, H.M. Ghasemi, R. Mahmudi, Wear, **292–293**, 33 (2012)
28. S. Tardif, R. Tremblay, D. Dubé, Mater. Sci. Eng., A **527**, 7519 (2010)
29. C.A.I. Huisheng, G.U.O. Feng, R.E.N. Xiushan, S.U. Juan, C. Baodong, J. Rare Earths **34**, 736 (2016)
30. T. Mukai, M. Yamanoi, H. Watanabe, K. Ishikawa, K. Higashi, Mater. Trans. **42**, 1177 (2001)
31. M. Faruk, A. OezDEMIR, K.U. Kainer, H. Norbert, Trans. Non-ferrous Met. Soc. China **23**, 66 (2013)
32. Z. Wang, J.G. Wang, Z.Y. Chen, M. Zha, C. Wang, S. Liu, R.F. Yan, Materials **12**, 76 (2018)
33. H. Yu, Y.M. Kim, B.S. You, H.S. Yu, S.H. Park, Mater. Sci. Eng., A **559**, 798 (2013)
34. K.H. Zum Gahr, *Microstructure and Wear of Materials* (Elsevier, New York, 1987), pp. 68–72
35. G.W. Stachowiak, A.W. Batchelor, *Engineering Tribology*, 4th edn. (Elsevier, New York, 2013), pp. 112–116
36. B. Bhushan, Tribol. Int. **36**, 559 (2001)
37. S. Garcia-Rodriguez, B. Torres, A. Maroto, A.J. Lopez, E. Otero, Wear **390–391**, 1 (2017)
38. W. Liu, F. Cao, L. Chang, Z. Zhang, J. Zhang, Corros. Sci. **51**, 1334 (2009)
39. M. Yang, X. Liu, Z. Zhang, Y. Song, L. Bai, Open Phys. **17**, 373 (2019)
40. J. Zhang, X. Niu, X. Qiu, K. Liu, C. Nan, D. Tang, J. Meng, J. Alloys Compd. **471**, 322 (2009)
41. Y. Han, Y. Xia, X. Chen, L. Sun, D. Liu, X. Ge, Anti-Corrosion Methods Mater. **65**, 131 (2018)

Publisher's Note Springer Nature remains neutral with regard to jurisdictional claims in published maps and institutional affiliations.